Detection of Onset of Melt and Freeze of Snow in the Upper Chenab Basin Using Remote Sensing Data

Ardra Santhosh[1], Vaibhav Garg[1], Praveen K. Thakur[1]

Water Resources Department, Indian Institute of Remote Sensing, 4, Kalidas Road, Dehradun – 248 001, Uttarakhand, India - ardrasanthosh88@gmail.com, (vaibhav, Praveen)@iirs.gov.in

Keywords: Backscatter, Albedo, Snow melt, Snow freeze, Google Earth Engine

Abstract

Snow cover and its changes play a significant role in influencing hydrological and climate processes. Each year, approximately one-third part of the land surface of earth undergoes seasonal snow coverage, highlighting its significant role as one of the most dynamic components of the cryosphere, alongside sea ice. In the cryosphere studies, identifying the onset and progression of snow accumulation and ablation is of utmost importance and critical significance. The present work highlights the importance of remote sensing (RS) data in detection and monitoring of melt and freeze of snow in different elevation zones in the Upper Chenab basin using synthetic aperture radar and albedo data along with temperature data . The detection of onset of melt and freeze of snow was carried out from 2015 to 2023. The optimal value for threshold was identified empirically by comparing air temperature time series data. The time series analysis of backscatter values and albedo values clearly depicts the melt and freeze of snow. As the surface air temperature increases above a particular value, there observed a consistent decrease in backscatter /albedo response. A short time delay in change in backscatter, albedo and temperature with the different elevation zones. As the temperature increases, the glacier starts melting and the water content increases, so the backscatter and albedo decreases and hence on the melting period the backscatter will be low and vice versa. Overall, the onset of melt of the snow will occur early in the lower elevation zone compared to the higher elevation zone. And the onset of freeze will occur early in the higher elevation zone compared to the lower elevation zone.

1. Introduction

Snow cover and its changes play a significant role in influencing hydrological and climate processes. Regions covered in snow exhibit a considerably higher albedo compared to bare terrain, which has a fundamental impact on atmospheric processes. Therefore, snow plays a vital role in climate modelling and weather forecasting, encompassing Earth system modelling and global circulation models (Takala et al., 2009). Each year, approximately one-third part of the land surface of earth undergoes seasonal snow coverage, highlighting its significant role as one of the most dynamic components of the cryosphere, alongside sea ice (Beltramone et al., 2023).In the cryosphere studies, identifying the onset and progression of snow accumulation and ablation is of utmost importance and critical significance (Beltramone et al., 2023). The cryosphere plays a crucial role on the production of hydroelectric power and the freshwater supply, which is mainly sourced from the seasonal melt of snow. Hydrologists concentrate on monitoring the seasonal snow accumulation and the subsequent extended melting period, which can span several months. The snow cover will persist as long as the atmosphere maintains freezing temperatures and high level of humidity. The Himalaya is often known as the “Third Pole,” and it hold the largest reservoir of snow and ice outside the polar regions in the world. The proper understanding about the dynamics of melt and freeze of snow cover is crucial in the field of hydrology, especially in the Himalayan region, as it serves as the source of ten major Asian river systems. Mainly, the Ganges, Indus, and Brahmaputra rivers significantly impact India by supplying water through snowmelt (Bothale et al., 2015). The presence of snow and ice is pivotal in modulating heating and cooling processes, thus impacting the energy balance within an environment. Alterations in snow conditions serve as markers of changing climate patterns. Snowmelt, in particular, is exceptionally sensitive to climate variations, notably warming trends. Furthermore, the snowmelt process significantly influences the broader dynamics of climate change, acting as a key contributing factor(Bothale et al., 2015). “Optical” and “Synthetic Aperture Radar (SAR)” satellite systems used for Earth observation offer unique advantages and disadvantages in glacier monitoring. Optical imagery is often utilized for mapping variables in glacier change studies, but its effectiveness is hindered in regions with mountainous terrain, maritime climates, and high latitudes due to presence of cloud cover and the polar night, which restrict the applicability of images. On the other hand, SAR instruments have the all-weather capability and can operate independently of solar radiation as active instruments, capable of penetrating through clouds. The combined use of SAR and optical imagery helps in understanding of glacier processes, providing complementary information that can lead to further advancements in glacier remote sensing applications (Winsvold et al., 2018). Monitoring and analysis of the radar backscatter is useful in identifying the onset of melting and freezing of snow. Panday et al., (2011) conducted an extensive study in the Himalayan and Karakoram regions, utilizing both seasonal snow cover and perennial snow/ice. They employed a dynamic threshold-based method on enhanced "QuikSCAT" Ku-band backscatter observations for a period of 2000 to 2008. This method aimed to (a) create spatial maps showing the onset of melt, freeze, and the duration of the melting, and (b) emphasize regional variations in freeze/thaw dynamics. Kimball et al., (2001) employed a temporal change detection analysis on daily radar backscatter data from NSCAT (NASA Scatterometer) to identify the surface freeze/thaw state across a vast region of Alaska, spanning 1.4 million km^2. The analysis covered the period from January to June 1997. Takala et al., (2009) employed four different algorithms to detect the date

of snowmelt using data from the “Scanning Multichannel Microwave Radiometer and Special Sensor Microwave/Imager”. These algorithms, were based on thresholding channel differences and employing neural networks, then uses time series analysis, were applied over a nearly 30-year period. Surdu et al., (2015) analysed the temporal data of C-band sigma naght backscatter coefficient (σ°) which is obtained from “Advanced Synthetic Aperture Radar (ASAR) Wide Swath” and “RADARSAT-2” scansar, which together provided the data at intervals ranging from two to five days and used these data to assess the ability of SAR in detecting the timing of important events related to lake-ice. In the Argentinean Andes, a novel method for recognising phase changes in seasonal snow cover was proposed and evaluated Beltramone et al., (2023).The researchers utilized time series data from the “Sentinel-1 SAR”, which is accessible through the Google Earth Engine platform. To validate the presence of snow, meteorological data and optical Sentinel-2 data were incorporated into their analysis. Kunz & Long, (2006) Used a method in which radar backscatter data of Ku-band dual-polarization from the “SeaWinds-on-QuikSCAT scatterometer” were utilized to determine surface melt and freeze periods in the ice shelves of Antarctic.

2. Study Area and dataset used

The Chandra Bhaga basin, located in the Lahul Spiti district of Himachal Pradesh, India, is bounded by 32° 05' 0" N to 32° 45' 0" N latitude and 76° 50' 0" E to 77° 50' 0" E longitude in the Western Indian Himalaya (Figure 1). Chandra and Bhaga are sub-basins of the Chenab basin covering an area of 4120 km^2 lying between the northern slopes of the Pir Panjal range and the southern slopes of the Great Himalayan range of the North-Western Indian Himalaya. The region is heavily glaciated with 736 km^2 glacial area in Chandra and 376 km^2 in Bhaga basin (Arendt et al., 2015). The elevation ranges from 2858 m to 6588 m above mean sea level. The Chandra and Bhaga rivers originate from the southwest and northwest faces, respectively of the Bara Lacha pass. Chandra River flows for ~125 km and Bhaga for ~80 km to reach their confluence point at Tandi, southwest of Keylong in the Lahaul and Spiti district of state HP, beyond which the river is named as Chandra-Bhaga or Chenab further downstream.

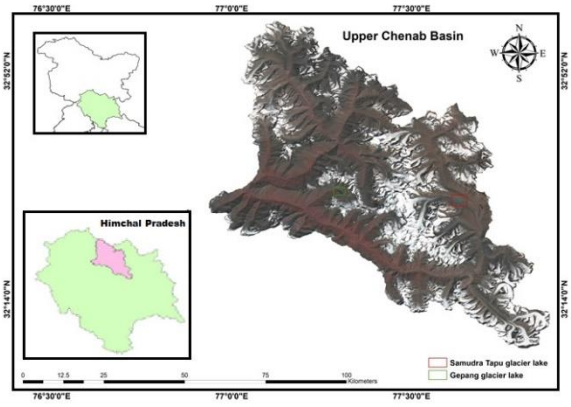

Figure 1 Location of Study Area

More than two hundred glaciers have been identified in this basin, of which 43 lies on its southern side (Pir-Panjal range) and flow into the mainstream of the Chandra-Bhaga River whereas on its northern side 157 glaciers of different orientations have been recognized flowing into the main river Chandra-Bhaga. The Chandra basin experience snowfall in the winter season (ONDJFM) and rainfall during the summer season (AMJJAS). Glaciers of Chandra basin gain mass because of the snowfall, avalanching and blowing snow. River Chandra originates from the Greater Himalayas and unites with River Bhaga at Tandi, Lahaul-Spiti, Himachal Pradesh. Bara Shigri is one of the largest glacier with 29 km length and 157 km^2 area in the Chandra basin. The other glaciers are SamudraTapu (18 km), Mulkila Gang (13.25 km), Chhota Shigri (9 km) Geepang Gath (5.5 km), Batal (6.3 km) and Miyar (25 km).

Of the 200 of the glaciers of the Chandra-Bhaga basin of Lahaul and Spiti District of Himachal Pradesh (Dobhal and Kumar, 1996), the Samudra Tapu Glacier is the second largest glacier of the upper Chandra basin after the Bara Shigri glacier. The region falls within the monsoon-arid transition zone, with a wet climate in the south-west with moderate precipitation in the form of rain and snow and a comparatively dry climate in the north-east with limited precipitation. The climate is influenced by western disturbances and extra-tropical cyclones that occur during October and May and south-west monsoons from July to September. The average precipitation and temperature according to monthly data from 1901 to 2001 are 63.9 mm and 8.9°C, respectively. The average monthly temperature varies from 16.8°C in July to -0.9°C in January.

Sl No	Remote sensing Data	Satellite/ Sensor	Spatial Resolution	Time Period	Data Source
1	Radar	Sentinel 1	10 m	2015-2023	https://scihub.copernicus.eu/
2	Snow Cover Product	MODIS	500 m	2015-2023	https://www.earthdata.nasa.gov/sensors/modis
3	Albedo product	MODIS	500 m	2015-2023	https://www.earthdata.nasa.gov/sensors/modis
4	DEM	NASADEM	30m		https://opentopography.org/

Table 1 Datasets Used

3. Methodology

The backscatter from snowpack changes significantly with variations in snow density, grain size, and particularly with liquid water content. Dry, dense snow with larger grains produces stronger backscatter. The presence of liquid water within the snowpack increases backscatter due to the higher dielectric constant, but excessive liquid water can lead to signal absorption and reduced backscatter. The detection of onset of melt and freeze of snow was carried out from 2015 to 2023. The onset of melt and freeze determined by the time series analysis of backscatter values of the “Sentinel 1 GRD” product of VV polarisation. Sentinel-1 has the advantage of providing the earth surface imagery in all weather conditions, day and night, and has a 06-day repeativity considering both ascending and descending pass, also it provides information in a variety of areas. The analysis of images from the “Sentinel-1 constellation”, including both “Sentinel-1A” and “Sentinel-1B”, was streamlined through the use of Google Earth Engine (GEE), which offers a repository of pre-processed Sentinel-1 images ready for analysis. These prepared images were derived by processing “Ground Range Detected (GRD)” Sentinel-1 images using the Sentinel-1

Toolbox by ESA (2018). This processing step involved generating calibrated and terrain-corrected images. For the study area and the study period, polarization with vertical transmission and vertical reception (VV) is used. GEE implements the following pre-processing steps to derive the backscatter coefficient in each pixel: apply orbit file, GRD border noise removal, thermal noise removal, radiometric calibration, terrain correction (orthorectification), and conversion to dB.

The DEM used was NASADEM of 30 m spatial Resolution. The DEM is reclassified into 9 Elevation zones in ArcMap with an interval of 500m as shown in Figure 2. The average backscatter value is extracted from each elevation zones only for the snow-covered area for a period from 2015 to 2023 for each Sentinel-1 image. The MODIS snow cover is used for masking out the non-snow pixels for the extraction of backscatter only for the snow pixels. The MODIS NDSI snow cover image corresponding to each Sentinel 1 image is used, as it is in dynamic nature. The extraction of backscatter is carried out with the help of Google Earth Engine. The onset of melt and freeze was determined based on a threshold-based approach. Sentinel-1 time series data exhibit a noticeable seasonal pattern, characterized by lower backscatter values during summer compared to winter. This decrease in backscatter intensity during summer is primarily attributed by the increased microwave absorption within a wet snowpack. Wet snow has a higher dielectric constant due to the presence of liquid water. This leads to increased absorption of microwave energy and less energy being reflected back to the satellite, resulting in lower backscatter values. The annual time series is divided into two distinct groups: one spanning from January to July and the other from July to December. These periods approximately correspond to the onset of melting and the freeze-up events, respectively, allowing for a comprehensive analysis of seasonal changes in backscatter behaviour. When the snow or glacier melt, the water content in the snow increases leading to the decreased backscatter. So, there is a gradual decrease in the backscatter and that drop indicate the melting of snow and similarly when the snow freeze there is a gradual increase in the backscatter coefficient values.

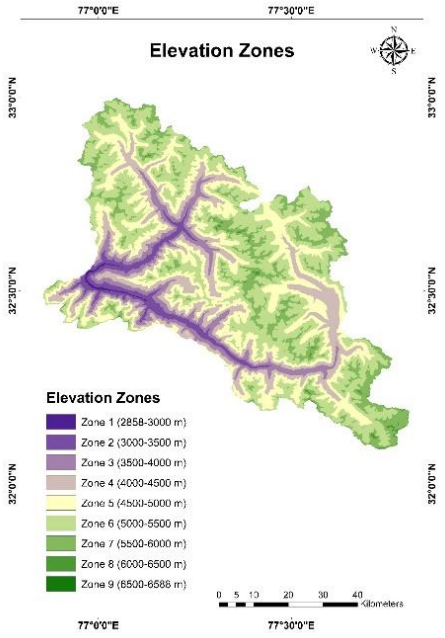

Figure 2 Map showing different elevation zones

This increase and decrease of backscatter value indicates the onset of melt and freeze, respectively. By analysing the backscatter values find out the threshold (b) below which there is melting and above which it is freezing. The optimal value for threshold was identified empirically by comparing air temperature time series data. The air temperature data was obtained from ERA5 reanalysis data for each elevation zones. ERA5 Land Hourly reanalysis data is used as the air temperature data. The pattern of temperature is opposite to that of backscatter. As temperature increases the snow and glacier starts to melt and when it decreases it freezes. Analysis of radar returns over time reveals a robust relationship between radar backscatter coefficient (σ°) and temperature. Generally, lower air temperatures are associated with higher σ° values, while higher air temperatures tend to result in decreased σ° values. So above a particular temperature it is said to melting season and below it is freezing. The methodology for detection of onset of melt and freeze is given as Figure 3.

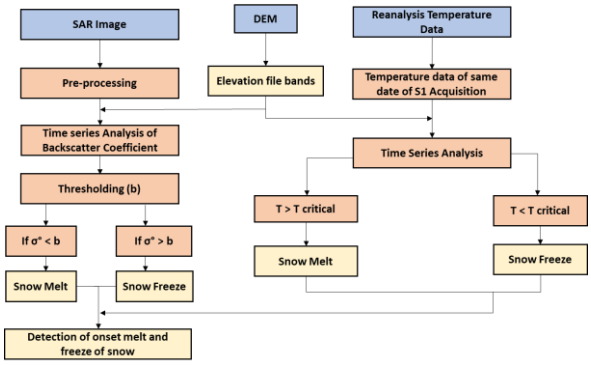

Figure 3 Methodology flowchart

4. Results and Discussion

In the present study, the onset of melt and freeze of snow and glacier was detected in the upper Chenab basin at different elevation zones from 2015 to 2023. The onset of melt and freeze was detected using the backscatter values of Sentinel-1 VV polarisation product. The time series analysis of backscatter values clearly depicts the melt and freeze of snow. As the surface air temperature increases above a particular value, a consistent increase in backscatter response also observed across the different elevation zones. As the temperature increases, the glacier starts melting and the water content increases, so the backscatter decreases and hence on the melting period the backscatter will be low and vice versa. A threshold-based approach is used for the detection of onset of melt and freeze. The study investigated the spatial variability of the average onset dates of snowmelt and freeze from 2015 to 2023, considering elevation differences across the study area. From these figures we can observe that the backscatter value is decreasing from the month of April, May and June and there is increase of the backscatter value from August, September, and October at different elevation zones. Figure 4 shows how the backscatter and temperature is varying in the elevation zone 7 for all the years from 2015 to 2023. From these graphs we can identify the backscatter threshold as -8 dB below which it is melting will occur and above that freezing will occur. These graphs clearly show the backscatter and temperature variation in a year and average value of the backscatter coefficient is found out from these graphs whenever the backscatter is decreasing, and air temperature is increasing or vice versa. This backscatter value is considered as the threshold for the detection of the onset of melt

and freeze. Based on the characteristics of melt and freeze of snow, we can divide the time series data into two, January to July and July to December.

Figure 4 Backscatter and Temperature variation for the zone 7 from 2025 to 2023

4.1 Detection of onset of melt using backscatter value

The detection of onset of melt and freeze is carried out in different zones based on the backscatter values and the temperature values. In the year 2015, the melt begins between March 19 and April 01 in the 4th elevation zone (4000 – 4500 m), between April 04 and April 24 in the 5th elevation zone (4500 – 5000 m), between April 13 and April 24 in the 6th elevation zone (5000-5500 m), between May 19 and May 23 in the 7th elevation zone (5500-6000 m), between May 19 and May 30 in the 8th elevation zone (6000-6500 m). In the year 2016, the melt begins between March 14 and April 07 in the 4th elevation zone (4000 – 4500 m), between April 07 and April 11 in the 5th elevation zone (4500 – 5000 m), between April 18 and May 05 in the 6th elevation zone (5000-5500 m), between May 01 and May 05 in the 7th elevation zone (5500-6000 m), between May 12 and May 29 in the 8th elevation zone (6000-6500 m). In the year 2017, the melt begins March 20 and April 01 between in the 4th elevation zone (4000 – 4500 m), between April 02 and April 06 in the 5th elevation zone (4500 – 5000 m), between April 14 and April 24 in the 6th elevation zone (5000-5500 m), between April 25 and May 07 in the 7th elevation zone (5500-6000 m), between May 12 and May 24 in the 8th elevation zone (6000-6500 m). The Figure 5 shows the spatial variation of melt onset in the year 2015 to 2017.

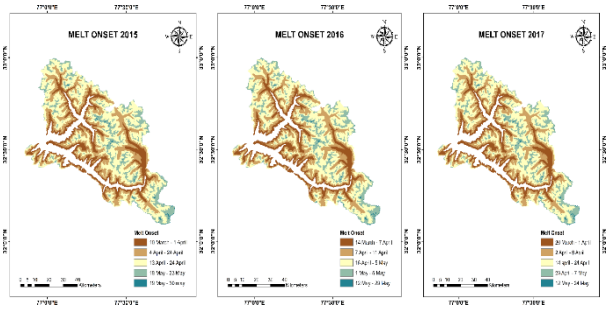

Figure 5 Spatial maps showing the melt onset at different elevation from 2015 -2017

In the year 2018 the melt begins between March 20 and April 01 in the 4th elevation zone (4000 – 4500 m), between April 01 and April 09 in the 5th elevation zone (4500 – 5000 m), between April 20 and April 25 in the 6th elevation zone (5000-5500 m), between May 19 and May 27 in the 7th elevation zone (5500-6000 m), between May 31 and June 07 in the 8th elevation zone (6000-6500 m). In the year 2019 the melt begins between March 23 and April 03 in the 4th elevation zone (4000 – 4500 m), between March 22 and March 27 in the 5th elevation zone (4500 – 5000 m), between April 27 and May 05 in the 6th elevation zone (5000-5500 m), between May 26 and June 07 in the 7th elevation zone (5500-6000 m), between June 03 and June 14 in the 8th elevation zone (6000-6500 m). In the year 2020 the melt begins between March 21 and March 28 in the 4th elevation zone (4000 – 4500 m), between April 02 and April 10 in the 5th elevation zone (4500 – 5000 m), between April 22 and May 05 in the 6th elevation zone (5000-5500 m), between May 08 and May 16 in the 7th elevation zone (5500-6000 m), between May 15 and May 27 in the 8th elevation zone (6000-6500 m). The Figure 6 shows the spatial variation of melt onset in the year 2018 to 2020.

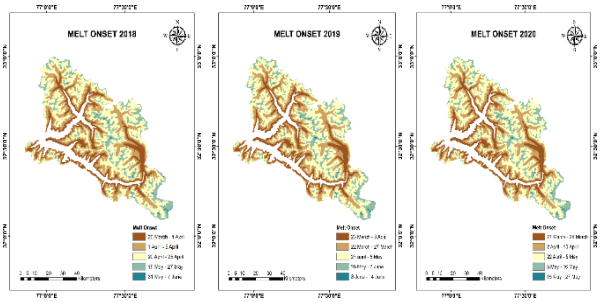

Figure 6 Spatial maps showing the melt onset at different elevation from 2018- 2020

In the year 2021 the melt begins between March 23 and March 28 in the 4th elevation zone (4000 – 4500 m), between April 16 and April 28 in the 5th elevation zone (4500 – 5000 m), between April 29 and May 03 in the 6th elevation zone (5000-5500 m), between May 23 and June 04 in the 7th elevation zone (5500-6000 m), between June 03 and June 08 in the 8th elevation zone (6000-6500 m). In the year 2022 the melt begins between March 31 and April 04 in the 4th elevation zone (4000 – 4500 m), between April 12 and April 16 in the 5th elevation zone (4500 – 5000 m), between April 23 and April 28 in the 6th elevation zone (5000-5500 m), between May 10 and May 18 in the 7th elevation zone (5500-6000 m), between June 15 and June 22 in the 8th elevation zone (6000-6500 m). In the year 2023 the melt begins between March 14 and March 25 in the 4th elevation zone (4000 – 4500 m), between April 07 and April 24 in the 5th elevation zone (4500 – 5000 m), between April 30 and May 13 in the 6th elevation zone (5000-5500 m), between May 24 and May 29 in the 7th elevation

zone (5500-6000 m), between May 25 and June 06 in the 8th elevation zone (6000-6500 m). The Figure 7 shows the spatial variation of melt onset in the year 2021 to 2023.

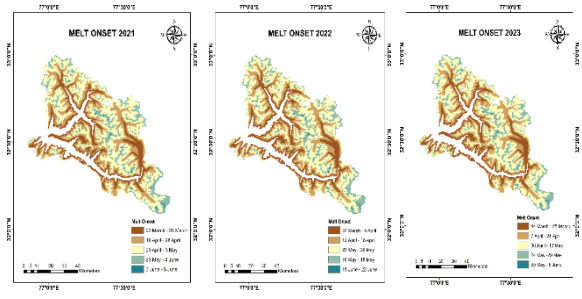

Figure 7 Spatial maps showing the melt onset at different elevation from 2021 - 2023

The average date of onset of melt is 26 March ± 7 days for the elevation zone 4, 11 April ± 6 days for the elevation zone 5, 25 April ± 7 days for the elevation zone 6, 19 May ± 11 days for the elevation zone 7 and 4 June ± 7 days for the elevation zone 8.

4.2 Detection of onset of freeze using backscatter value

In the year 2015 the freeze begins between September 28 and October 02 in the 4th elevation zone (4000 – 4500 m), between September 16 and September 28 in the 5th elevation zone (4500 – 5000 m), between September 28 and October 02 in the 6th elevation zone (5000-5500 m), between August 27 and September 03 in the 7th elevation zone (5500-6000 m), between August 27 and September 03 in the 8th elevation zone (6000-6500 m). In the year 2016 the freeze begins between October 04 and October 10 in the 4th elevation zone (4000 – 4500 m), between October 04 and October 10 in the 5th elevation zone (4500 – 5000 m), between September 28 and October 03 in the 6th elevation zone (5000-5500 m), between September 26 and October 03 in the 7th elevation zone (5500-6000 m), between September 26 and September 28 in the 8th elevation zone (6000-6500 m). In the year 2017 the freeze begins between 03 October and 22 October in the 4th elevation zone (4000 – 4500 m), between October 03 and October 15 in the 5th elevation zone (4500 – 5000 m), between September 29 and October 10 in the 6th elevation zone (5000-5500 m), between September 09 and September 16 in the 7th elevation zone (5500-6000 m), between September 05 and September 17 in the 8th elevation zone (6000-6500 m). The Figure 8 shows the spatial variation of freeze onset in the year 2015 to 2017.

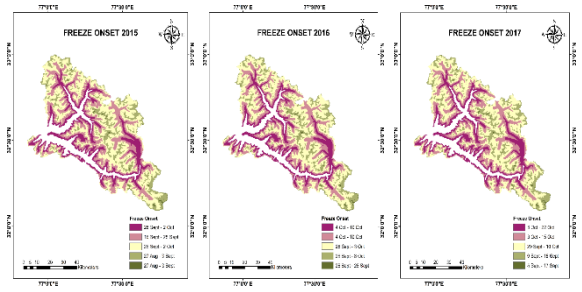

Figure 8 Spatial maps showing the freeze onset at different elevation from 2015-2017

In the year 2018 the freeze begins between September 24 and 06 October in the 4th elevation zone (4000 – 4500 m), between September 23 and September 28 in the 5th elevation zone (4500 – 5000 m), between September 16 and September 23 in the 6th elevation zone (5000-5500 m), between September 12 and September 16 in the 7th elevation zone (5500-6000 m), between September 04 and September 12 in the 8th elevation zone (6000-6500 m). In the year 2019 the freeze begins between October 05 and October 12 in the 4th elevation zone (4000 – 4500 m), between September 30 and October 05 in the 5th elevation zone (4500 – 5000 m), between September 23 and October 05 in the 6th elevation zone (5000-5500 m), between September 19 and September 23 in the 7th elevation zone (5500-6000 m), between September 11 and September 19 in the 8th elevation zone (6000-6500 m). In the year 2020 the freeze begins between October 19 and October 23 in the 4th elevation zone (4000 – 4500 m), between September 29 and October 07 in the 5th elevation zone (4500 – 5000 m), between September 25 and September 29 in the 6th elevation zone (5000-5500 m), between September 17 and September 25 in the 7th elevation zone (5500-6000 m), between September 13 and September 24 in the 8th elevation zone (6000-6500 m). The Figure 9 shows the spatial variation of freeze onset in the year 2018 to 2020.

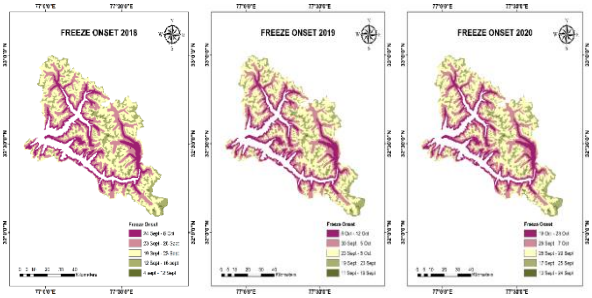

Figure 9 Spatial maps showing the freeze onset at different elevation from 2018-2020

In the year 2021 the freeze begins between October 18 and October 26 in the 4th elevation zone (4000 – 4500 m), between October 13 and October 18 in the 5th elevation zone (4500 – 5000 m), between October 02 and October 14 in the 6th elevation zone (5000-5500 m), between September 24 and September 02 in the 7th elevation zone (5500-6000 m), between September 24 and September 02 in the 8th elevation zone (6000-6500 m). In the year 2022 the freeze begins between October 08 and October 20 in the 4th elevation zone (4000 – 4500 m), between October 01 and October 08 in the 5th elevation zone (4500 – 5000 m), between October 01 and October 08 in the 6th elevation zone (5000-5500 m), between September 19 and September 26 in the 7th elevation zone (5500-6000 m), between September 07 and September 14 in the 8th elevation zone (6000-6500 m). In the year 2023 the freeze begins between October 20 and November 01 in the 4th elevation zone (4000 – 4500 m), between October 08 and October 16 in the 5th elevation zone (4500 – 5000 m), between September 26 and October 03 in the 6th elevation zone (5000-5500 m), between September 21 and September 26 in the 7th elevation zone (5500-6000 m), between September 14 and September 21 in the 8th elevation zone (6000-6500 m). The Figure 10 shows the spatial variation of freeze onset in the year 2021 to 2023.

The average date of freeze-up is 13 October ± 4 days for the elevation zone 4, 05 October ± 4 days for the elevation zone 5, 1 October ± 3 days for the elevation zone 6, 23 September ± 7 days for the elevation zone 7 and 11 September ± 7 days for the elevation zone 8.

At lower elevation the onset of melt is occurring early (late march/early April) and at higher elevation it is occurring late (late

May/early June). Whereas at lower elevation the onset of freeze is occurring late (in October) and at higher elevation it is occurring early (in September). So, the no of melt days will be more in the lower elevation than the higher elevation.

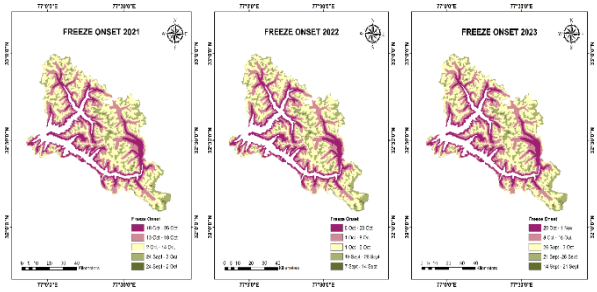

Figure 10 Spatial maps showing the freeze onset at different elevation from 2021-2023

4.3 Detection of Melt and Freeze using Modis Albedo

Fresh snow has a high value of albedo, meaning a large portion of the incoming solar radiation is reflected by the snow. Surface albedo undergoes significant changes with snowfall and aging. Fresh snow typically has a high albedo ranging from 0.8 to 0.9, which gradually decreases as the snow becomes wetter and more uneven. Dense, dry, and clean snow has the highest albedo of around 0.9, while damp and dirty snow exhibit lower albedo values, ranging from 0.3 to 0.6 (Li et al., 2023). As snow begins to melt, its surface becomes wetter and less reflective, causing the albedo to decrease. By monitoring changes in albedo values over time, particularly in areas where snow cover is present, it is possible to track the onset of snowmelt. When the albedo of a snow-covered area begins to decrease, it indicates that the snowpack is starting to melt. Conversely, as temperatures drop and the melted snow refreezes, the surface becomes drier and more reflective, causing the albedo to increase again. Monitoring these increases in albedo can indicate the onset of the refreezing process.

The Figure 11 depicts the albedo and backscatter variation at different elevation zone for the year 2015. Similar to the backscatter value the albedo value also decreases as the melting of snow starts. It starts decrease from the value 0.8 and reach up to 0.4. So, by using the albedo value also we can detect the timing of melt and freeze of snow, and it can be used as complementary along with the backscatter. The Figure 12 and 13 shows the spatial maps showing the onset of melt and freeze of snow at all elevation zones for the period from 2015 to 2022 respectively. We used the daily MODIS albedo of 500 m spatial resolution. Albedo is a measure of how much sunlight is reflected by a surface. From these graphs also we can say that the albedo value is decreasing which indicates the melting of snow and it increases when snow starts to freeze.

4.4 Comparison of onset dates detected by SAR and albedo values

In analysing the onset date of snowmelt using SAR data and MODIS albedo data, a discrepancy of 15 to 20 days was observed. Specifically, SAR data indicates an earlier onset of melt compared to the MODIS albedo data. This difference can be explained by the distinct sensitivities of these two remote sensing technologies to snow properties (Lund et al., 2022). The SAR data is highly sensitive to changes in the dielectric properties of the snowpack, which occur as soon as liquid water begins to form within the snow. This early detection is possible because SAR can penetrate the snowpack and detect internal changes, such as the initial melting of ice crystals and the formation of liquid water. As a result, SAR identifies the onset of melt as soon as these internal processes begin, even before significant surface melt is visible. In contrast, MODIS albedo data relies on measuring the reflectivity of the snow surface. Albedo decreases as the snow begins to melt and the surface becomes less reflective. However, this change in albedo is often delayed compared to the internal melt detected by SAR because it requires a significant amount of surface melting for the reflectivity to noticeably decrease. The surface melt needs to be substantial enough to alter the snow cover characteristics, which can take additional time after the initial internal melting has started. Thus, the earlier onset date detected by SAR data captures the initial stages of internal snowmelt, while the later date from MODIS albedo data represents more pronounced surface changes. This difference highlights the complementary nature of using both SAR and albedo data to gain a comprehensive understanding of snowmelt processes. SAR's sensitivity to internal changes and MODIS's reliance on surface reflectivity provide a broader perspective on the timing and progression of snowmelt, ultimately offering more detailed insights into these complex environmental phenomena. In analysing the onset date of freeze using MODIS albedo data and SAR data, a discrepancy was observed, with albedo data indicating an earlier onset of freeze compared to SAR data. This difference can be attributed to the distinct sensitivities of these remote sensing technologies. MODIS albedo data, which measures surface reflectivity, detects freeze onset earlier because the surface becomes more reflective as soon as liquid water begins to refreeze. In contrast, SAR data, which is sensitive to internal changes within the snowpack, indicates freeze onset later by detecting changes in the backscatter signal due to the formation of ice crystals and the reduction of liquid water content. Thus, the albedo data captures immediate surface changes, while SAR data detects subsequent internal refreezing, highlighting the complementary nature of using both methods for a comprehensive understanding of the freeze process.

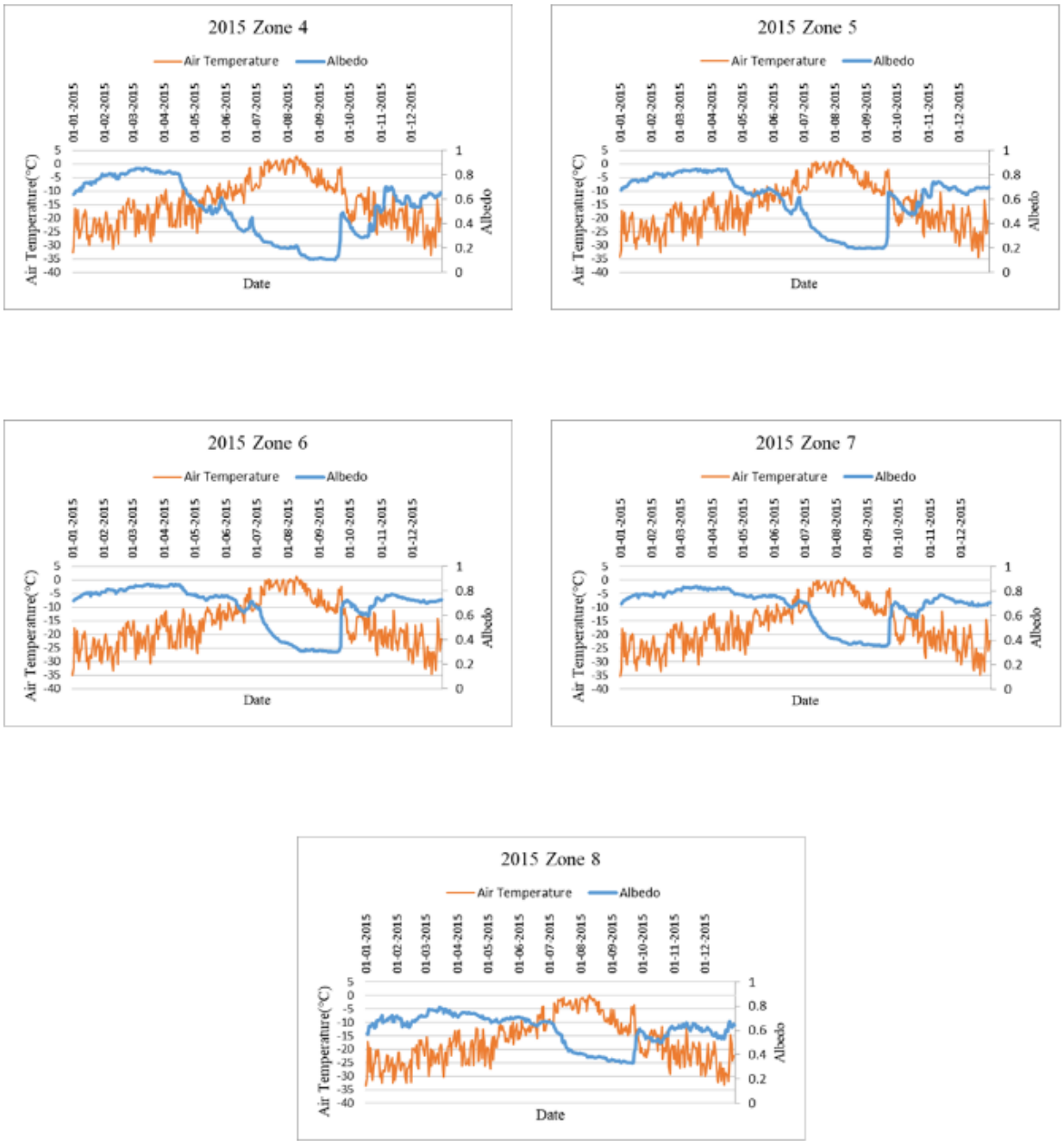

Figure 11 Albedo and Temperature variation for the year 2015 for different elevation zones

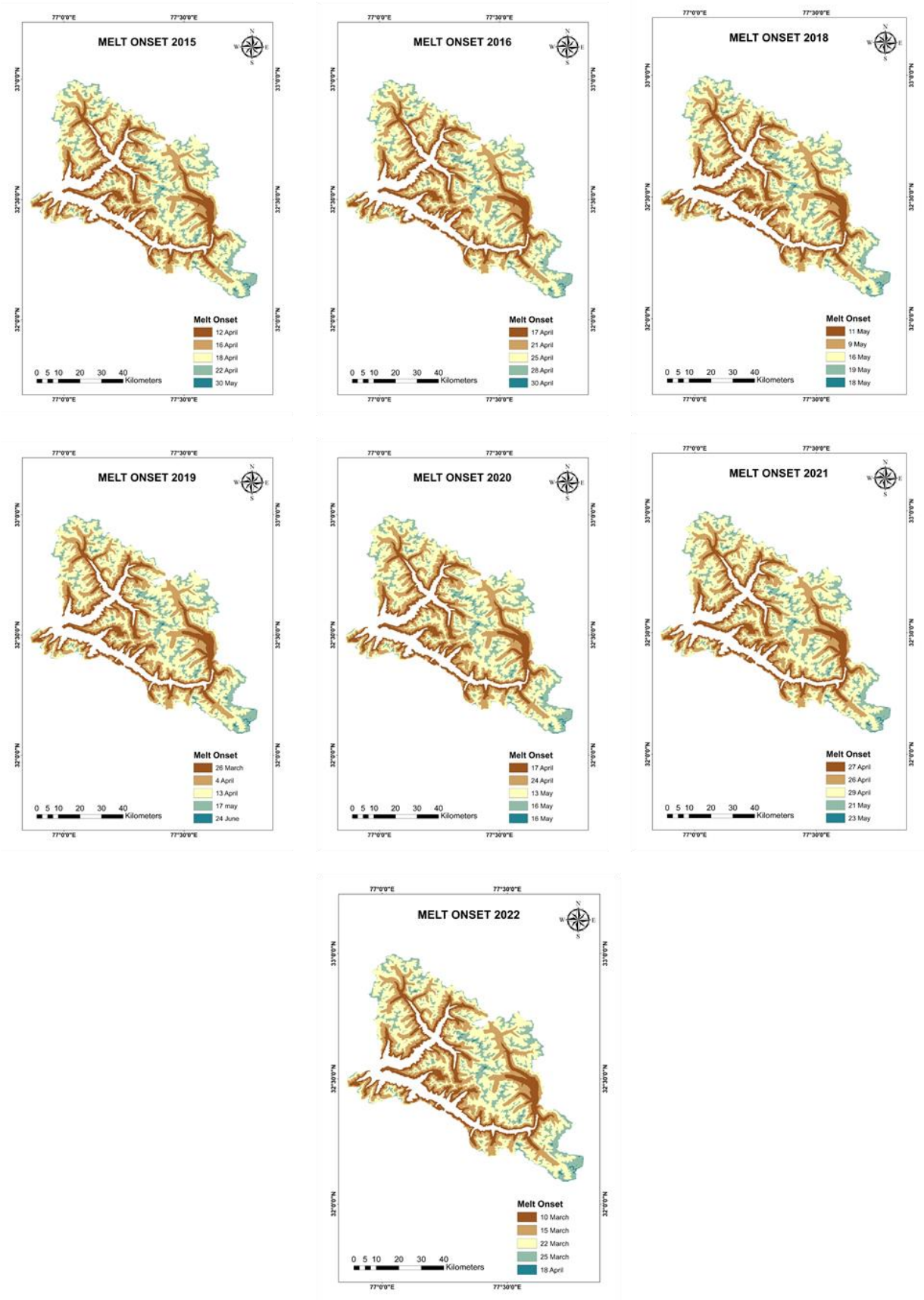

Figure 12 Spatial maps showing the melt onset at different elevation from 2015-2022

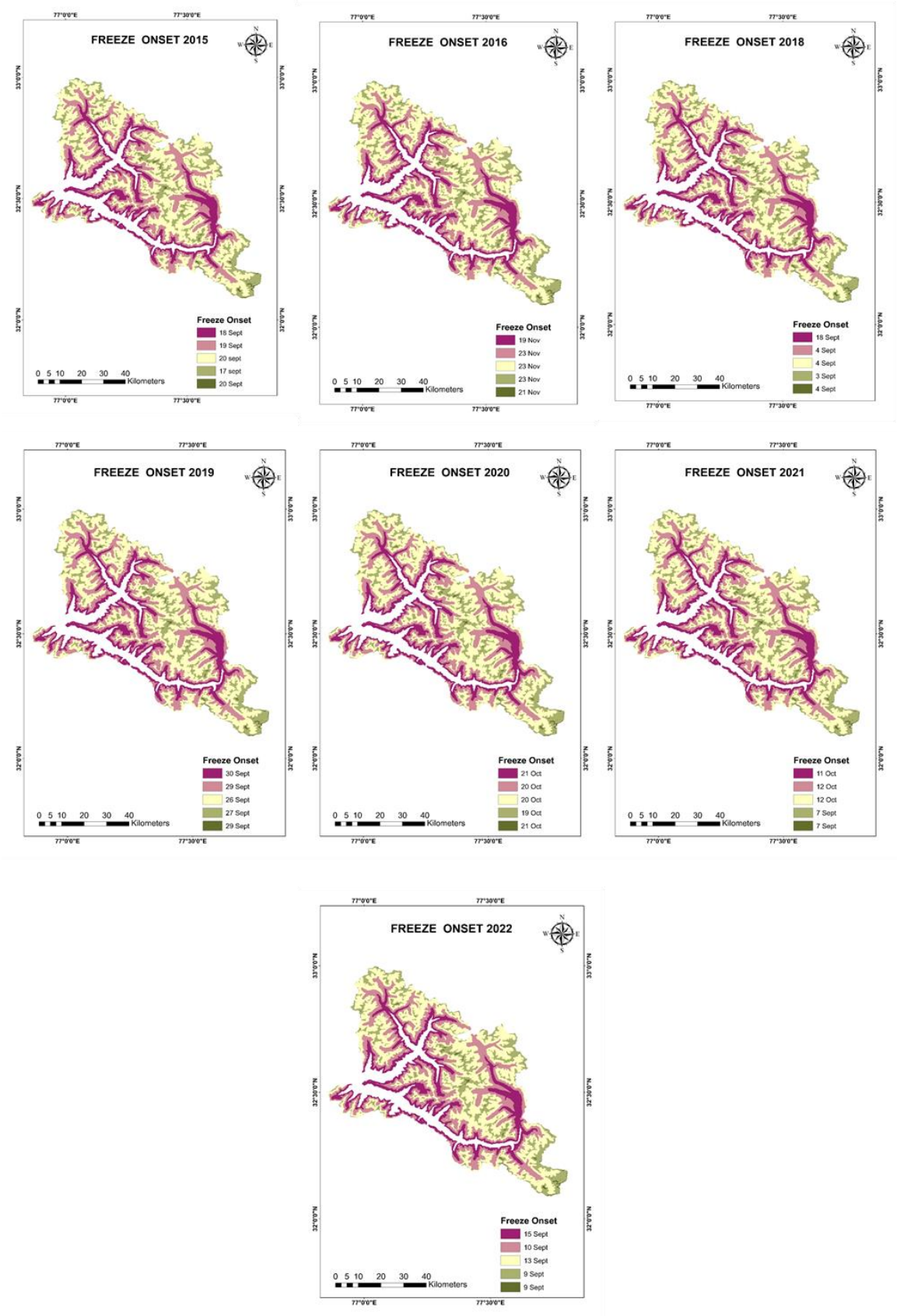

Figure 13 Spatial maps showing the freeze onset at different elevation from 2015-2022

5. Conclusions and Recommendation

The study provides the change in the onset of melt and freeze with varying elevation from the year 2015 and 2023. The onset of melt and freeze in the snow-covered areas of each elevation zone was detected by using the time series analysis of the Sentinel-1 data for the period of 2015 to 2023. The use of snow cover data corresponding to each Sentinel-1 image made the results made the results more reliable. The average backscatter value is extracted from each elevation zones only for the snow-covered area for a period from 2015 to 2023 for each Sentinel-1 image. The MODIS snow cover is used as the snow mask for the extraction of backscatter for the snow pixels. The average date of onset of melt is 26 March ± 7 days for the elevation zone 4, 11 April ± 6 days for the elevation zone 5, 25 April ± 7 days for the elevation zone 6, 19 May ± 11 days for the elevation zone 7 and 04 June ± 7 days for the elevation zone 8 and the average date of freeze-up is 13 October ± 4 days for the elevation zone 4, 05 October ± 4 days for the elevation zone 5, 01 October ± 3 days for the elevation zone 6, 23 September ± 7 days for the elevation zone 7 and 11 September ± 7 days for the elevation zone 8. In analysing the onset date of snowmelt using Synthetic Aperture Radar (SAR) data and MODIS albedo data, a discrepancy of 15 to 20 days was observed. Specifically, SAR data indicates an earlier onset of melt compared to the MODIS albedo data. This difference can be explained by the distinct sensitivities of these two remote sensing technologies to snow properties. By analysing the variations in backscatter from radar data and albedo from optical measurements, we identified clear patterns corresponding to the phases of snowmelt and refreezing. The integration of these remote sensing techniques provided a robust approach to monitor snow dynamics, offering a significant advantage over traditional ground-based methods. Our findings reveal that the backscatter values exhibit a marked decrease during the onset of melt due to the increase in liquid water content within the snowpack. Conversely, the albedo values decrease as the snow begins to melt, reflecting the surface’s reduced reflectivity. During the refreezing phase, backscatter values increase, indicating the formation of ice layers, while albedo values stabilize as the snow surface refreezes. This methodology not only enhances our understanding of snowmelt and freeze processes but also offers valuable insights for hydrological modelling, climate studies, and water resource management. Future research could further refine these techniques by incorporating higher temporal and spatial resolution data, as well as integrating additional remote sensing parameters to improve the accuracy and reliability of snow condition monitoring. In conclusion, the use of backscatter and albedo values provides a powerful, non-invasive means to monitor and predict snowmelt and freeze cycles, thereby contributing significantly to our ability to manage and respond to changing snow conditions in a warming climate.

References

Beltramone, G., Frery, A. C., Rotela, C., German, A., Bonansea, M., Scavuzzo, C. M., & Ferral, A. (2023). Identification of Seasonal Snow Phase Changes from C-band SAR Time Series with Dynamic Thresholds. IEEE Journal of Selected Topics in Applied Earth Observations and Remote Sensing, 16, 6995–7008. https://doi.org/10.1109/JSTARS.2023.3281149

Bothale, R. V., Rao, P. V. N., Dutt, C. B. S., & Dadhwal, V. K. (2015). Detection of snow melt and freezing in Himalaya using OSCAT data. Journal of Earth System Science, 124(1), 101–113. https://doi.org/10.1007/s12040-014-0524-y

Kimball, J. S., McDonald, K. C., Keyser, A. R., Frolking, S., & Running, S. W. (2001). Application of the NASA scatterometer (NSCAT) for determining the daily frozen and nonfrozen landscape of Alaska. Remote Sensing of Environment, 75(1), 113–126. https://doi.org/10.1016/S0034-4257(00)00160-7

Kunz, L. B., & Long, D. G. (2006). Melt detection in antarctic ice shelves using scatterometers and microwave radiometers. IEEE Transactions on Geoscience and Remote Sensing, 44(9), 2461–2468. https://doi.org/10.1109/TGRS.2006.874138

Lund, J., Forster, R. R., Deeb, E. J., Liston, G. E., Skiles, S. M. K., & Marshall, H. P. (2022). Interpreting Sentinel-1 SAR Backscatter Signals of Snowpack Surface Melt/Freeze, Warming, and Ripening, through Field Measurements and Physically-Based SnowModel. Remote Sensing, 14(16). https://doi.org/10.3390/rs14164002

Panday, P. K., Frey, K. E., & Ghimire, B. (2011). Detection of the timing and duration of snowmelt in the Hindu Kush-Himalaya using QuikSCAT, 2000-2008. Environmental Research Letters, 6(2), 2000–2008. https://doi.org/10.1088/1748-9326/6/2/024007

Surdu, C. M., Duguay, C. R., Pour, H. K., & Brown, L. C. (2015). Ice freeze-up and break-up detection of shallow lakes in Northern Alaska with spaceborne SAR. Remote Sensing, 7(5), 6133–6159. https://doi.org/10.3390/rs70506133

Takala, M., Pulliainen, J., Metsamaki, S. J., & Koskinen, J. T. (2009). Detection of snowmelt using spaceborne microwave radiometer data in Eurasia from 1979 to 2007. IEEE Transactions on Geoscience and Remote Sensing, 47(9), 2996–3007. https://doi.org/10.1109/TGRS.2009.2018442

Winsvold, S. H., Kääb, A., Nuth, C., Andreassen, L. M., Van Pelt, W. J. J., & Schellenberger, T. (2018). Using SAR satellite data time series for regional glacier mapping. Cryosphere, 12(3), 867–890. https://doi.org/10.5194/tc-12-867-2018